STUDY ON MECHANICAL CHARACTERISTICS OF ROCK TYPE I FRACTURE AND ANCHORAGE STRENGTHENING MECHANISM

WEI ZHANG, TONGBIN ZHAO, WEIYAO GUO, MINGLU XING

State Key Laboratory of Mining Disaster Prevention and Control Co-founded by Shandong Province and the Ministry of Science and Technology, Shandong University of Science and Technology, Qingdao, China, and

College of Energy and Mining Engineering, Shandong University of Science and Technology, Qingdao, China

Corresponding author Tongbin Zhao, e-mail: 1125671372@qq.com

Engineering rocks are easily affected by excavation unloading and are in uniaxial compression or tension, forming a typical I-type tension crack. Anchor rods are often used for on-site support to ensure safety and reliability of the project. The study of propagation and penetration of type I tension cracks and quantitative evaluation of rock anchoring effects are of great significance for exploring mechanical properties of rock fracture and revealing the mechanism of rock failure. In this paper, combined with speckle light measurement, a rock fracture toughness test of different anchoring positions and pre-tightening forces is carried out, the deformation evolution law of the crack tip and the fracture mechanics characteristics of the anchored rock are obtained, and the anchoring strengthening mechanism of the rock is discussed based on the theory of the net stress intensity factor. The research shows that the rock fracture process is divided into four stages: elastic deformation, steady crack propagation, crack instability propagation and residual deformation. After anchoring, the time of crack instability growth can be prolonged by 172% and the final residual deformation can be increased by 148%. Compared with the unanchored rock, the fracture toughness of rock initiation and instability increased by 83% and 124% respectively, and increased with growth of the pre-tightening force, which shows that the bolt increases the critical value of rock initiation and instability to achieve the toughening effect. After the rock is anchored, the time required for the crack to propagate to the same length increases by 55%, and the lateral deformation area is reduced by 46%, indicating that the lateral closing force of the bolt inhibits crack propagation and delays the instability of the rock matrix.

Keywords: anchor rock, fracture type of I, fracture toughness, three-point bending test, toughening

1. Introduction

Rock is a special kind of are engineering medium material, showing complex characteristics such as discontinuity and heterogeneity. Propagation and penetration of internal cracks are important factors that cause overall failure and instability (Shu *et al.*, 2019). Under the action of structural and self-weight stress in engineering rock mass, the tip of the internal crack often appears in a compression-shear state, and when the stress intensity factor reaches a critical value, a typical I-type tensile crack is formed (Olsson *et al.*, 2019). Chinese and foreign scholars fully studied the tensile growth behavior of rock cracks under compressive and shear stress, and found that the micro-cracks basically form type I fracture cracks (Wang and Su, 2019). Type II and type III cracks are essentially secondary phenomena in the growth process of type I cracks. Therefore, studying the propagation and penetration characteristics of mode I cracks in rock is of great significance to the study of the rock failure mechanism, determining the path of rock crack propagation and the location of the failure surface, etc.

The instability and failure of rock under load is closely related to the evolution of mode I cracks. The application of theory of rock fracture mechanics to the reinforcement research of rock engineering has an important theoretical and engineering guiding significance for exploring the fracture law and anchoring characteristics of rock materials. Fracture toughness can quantitatively describe the steady state and instability propagation process of cracks, cover the initiation and instability conditions of rock masses, and can be used as an important index for evaluating rock mass engineering stability (Parisio *et al.*, 2019). At present, the International Society of Rock Mechanics (ISRM) has proposed four common methods for measuring the fracture toughness of rock I cracks: the V-grooved short round bar specimen (SR), V-grooved three-point bending round beam specimen (CB), V type grooved Brazilian disc specimen (CCNBD) and the single-sided straight crack three-point bending beam specimen (SC3PB) (Jenabidehkordi, 2019). The statistical results of the above-mentioned recommended test methods are all within a reasonable error range, and are recognized as the standard for rock fracture toughness testing (Pakdaman *et al.*, 2019). Compared with the other three samples, the straight-crack rectangular cross-section beam sample is simple in shape and easy to prepare, which has lower requirements for experimental equipment and materials, and has been widely recognized by the rock mechanics community (Nejati *et al.*, 2019).

In view of the fracture toughness test of rock type I cracks, Funatsu *et al.* (2004) studied fracture characteristics of Kinachi sandstone under different temperature conditions through a three-point bending test of pre-cracked rectangular cross-section beams with straight cracks. Zuo *et al.* (2013a,b) conducted three-point bending fracture failure tests of granite and basalt, and obtained fracture failure characteristics and crack propagation laws of rocks in different depth ranges, and revealed the mechanism of rock burial depth on its fracture mechanical properties. Deng *et al.* (2016, 2017) conducted three-point bending tests on four granites with different grain sizes and two diorites with different water content. Combining corresponding acoustic emission characteristics, they discussed fracture characteristics of different types of rocks. The results show that the acoustic emission event distribution of the finer rock during the fracture process is closer to the lower part of the main fracture surface, and the ringing count rate of the saturated specimen is much lower than that of the dry specimen.

The above research results have improved the understanding of fracture characteristics of rock materials under the action of three-point bending. Considering that the evolution of the deformation field at the tip of type I fracture crack is the key research object of the rock fracture process. The obtaining of meso-scale rock fracture characteristics has an important theoretical significance for in-depth understanding of the rock fracture mechanism. Digital Speckle Correlation Method (DSCM) gives characteristics from full-field measurement and non-contact, and has significant advantages in studying rock fracture characteristics and crack propagation laws (Wu *et al.*, 2002). Dai *et al.* (2012) used DSCM to determine the position of the granite crack tip and the stress intensity factor, revealing the characteristics of crack propagation and evolution during rock fracture. Ma and Zhou (2008) used DSCM to study the evolution process of the deformation field during the uniaxial compression failure of a central round hole rock, and obtained the law of deformation concentration at different load levels. Ji *et al.* (2016) obtained the critical deformation field of rock fracture and determined the length of the process zone of rock failure through DSCM.

2.   Three-point bending test of pre-cracked red sandstone

2.1.   Determination of rock fracture mechanics parameters

According to the existing rock fracture toughness determination method, comprehensive consideration of the factors influencing specimen preparation and anchoring conditions, single-

-sided straight crack three-point bending is used to test the fracture toughness of unanchored and anchored rocks. The main research parameters include crack initiation fracture toughness K_{Ic}^{ini} and instability fracture toughness K_{Ic}^{un}.

2.1.1. Determination of initiation load and instability load

During the initiation of rock, the tensile strain at the crack tip continues to increase. The crack tip would crack when the tensile strain reaches the peak. After the initiation, the energy accumulated on both sides of the crack tip is released, the strain will gradually decrease, and an even compressive strain will appear (Aliha and Saghafi, 2013). As shown in Fig. 1a, the curve of P-ε (P – external load, kN; ε – transverse strain) shows a process where the strain firstly rises and then falls with the load. When the strain begins to fall, the corresponding load is the crack initiation load. The instability load can be obtained from the peak point of the P-$CMOD$ ($CMOD$ – crack opening displacement, mm) curve, and the crack opening displacement corresponding to the maximum load is the critical opening displacement $CMOD_c$, as shown in Fig. 1b.
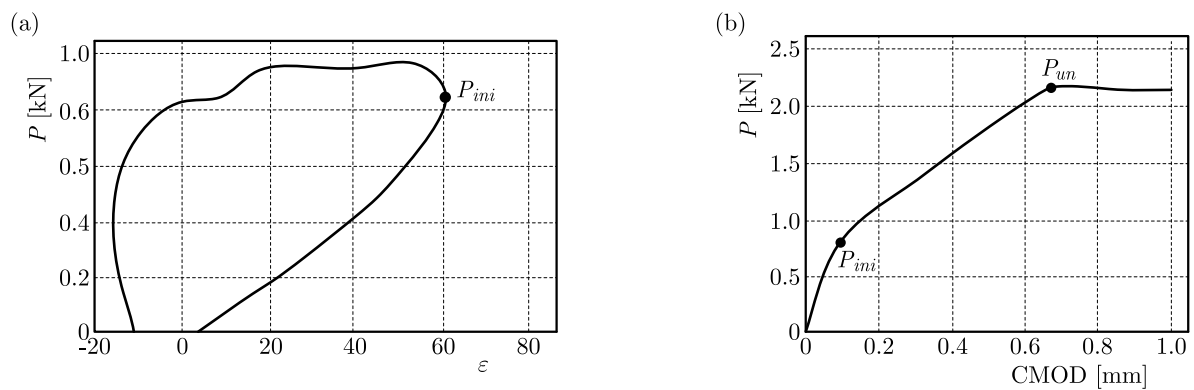

Fig. 1. The curve of: (a) P-ε (a) and (b) P-$CMOD$

2.1.2. Calculation of effective crack length

According to the empirical formula for calculating the effective crack length in literature (Aliha *et al.*, 2016)

$$a = \frac{2}{\pi}(h + H_0)\arctan\sqrt{\frac{EtCMOD}{\beta P} - \frac{\alpha}{\beta}} - H_0 \tag{2.1}$$

In formula (2.1), h is height of the specimen, mm; t is thickness of the specimen, mm; H_0 is width of the pre-crack, mm; α and β are empirical coefficients. According to the literature (Aliha *et al.*, 2016), $\alpha = 3.7$, $\beta = 32.6$, formula (2.1) can be converted to

$$a = \frac{2}{\pi}(h + H_0)\arctan\sqrt{\frac{Et}{32.6P}CMOD - 0.1135} - H_0 \tag{2.2}$$

Substituting H_0, h, t and the measured $CMOD_c$ and P_{un} into formula (2.2), one can obtain a_c.

2.1.3. Calculation of initiation fracture toughness and instability fracture toughness

The ASTM recommended formula (Ding *et al.*, 2013) is used to calculate the stress intensity factor

$$K_{Ip} = \frac{PS}{h^{1.5}t}F_1\left(\frac{a}{h}\right) \tag{2.3}$$

Among formula (2.3)

$$F_1\left(\frac{a}{h}\right) = 2.9\left(\frac{a}{h}\right)^{0.5} - 4.6\left(\frac{a}{h}\right)^{1.5} + 21.8\left(\frac{a}{h}\right)^{2.5} - 37.6\left(\frac{a}{h}\right)^{3.5} + 38.7\left(\frac{a}{h}\right)^{4.5} \qquad (2.4)$$

In formula (2.4), S is span, mm; a is real-time crack length, mm.

Under the action of the load P, the three-point bending beam bears all the external loads by the structure itself. Substituting the cracking load P_{ini} and the initial crack length a_0 into formula (2.3), one can obtain the cracking fracture toughness K_{Ic}^{ini}. The instability load P_{un} and the critical effective crack length a_c are substituted into formula (2.3) to obtain the instability fracture toughness K_{Ic}^{un}.

2.2. Specimen model and preparation

The red sandstone used in this paper is taken from the mining area in eastern China, and the main chemical composition is listed in Table 1.

Table 1. Chemical composition of red sandstone

Lithology	SiO_2 [%]	Al_2O_3 [%]	Fe_2O_3 [%]	CaO [%]	MgO [%]
Red sandstone	$\geqslant 35$	$\leqslant 44$	$\leqslant 3$	$\leqslant 2$	$\leqslant 1$

Combining the fracture parameters of concrete standard specimens proposed by the International Union of Laboratories and Experts in Construction Materials (IULECM) (Tada *et al.*, 2000), and recommendations for the specimen size and pre-crack length in "Recommended Method for Rock Fracture Toughness Testing (Straight-Notch Three-Point Bending Beam)" (Hu *et al.*, 2011), taking into account the convenience of anchoring drilling and the rationality of the digital speckle method, a three-point bending specimen with size $l \times$ width $t \times$ height h is $150\,\text{mm} \times 30\,\text{mm} \times 30\,\text{mm}$ is determined, and the notch crack with a length of 10mm is pre-fabricated at the mid-span in the longitudinal direction. The initial crack width $w = 2\,\text{mm}$ is shown in Fig. 2a. In rock type I fracture, the anchor rod perpendicular to the crack surface has the best reinforcement effect (Xu and Reinhardt, 2000), so the anchoring specimen adopts the transverse anchoring method perpendicular to the pre-crack, as shown in Fig. 2b. The size of the anchored specimen is the same as that of the unanchored comparison specimen, and the span S is $120\,\text{mm}$, among which 3 unanchored specimens are made for comparison.
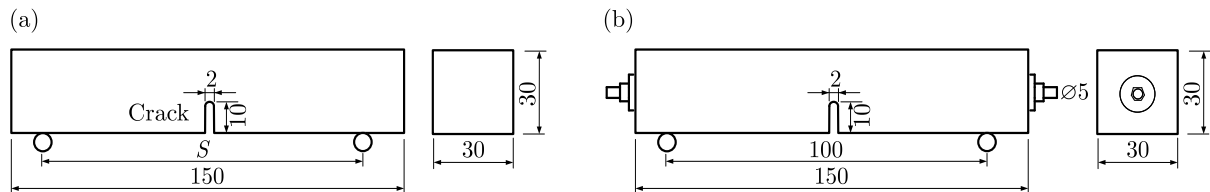

Fig. 2. Three-point bending specimen [mm]: (a) unanchored specimen, (b) anchored specimen

When preparing the anchored specimen, firstly drill a 5 mm diameter through hole in the original rock, then use emery wire to make a pre-crack with a width of 2 mm, and finally perforate the anchor rod and fasten it with nuts and washers. The anchor rod adopts a 6.8 grade stainless steel wire threaded rod with a diameter of 5 mm, and the tray uses a galvanized carbon steel gasket with an outer diameter of 30 mm and a thickness of 3 mm, which is shown in Fig. 3. The parallelism deviation of the upper and lower ends of the processed specimen is controlled within 0.05 mm, the size deviation of the upper and lower ends and the left and right ends of the test piece are all less than 0.1 mm, and the left and right ends of the specimen are perpendicular to the horizontal axis.
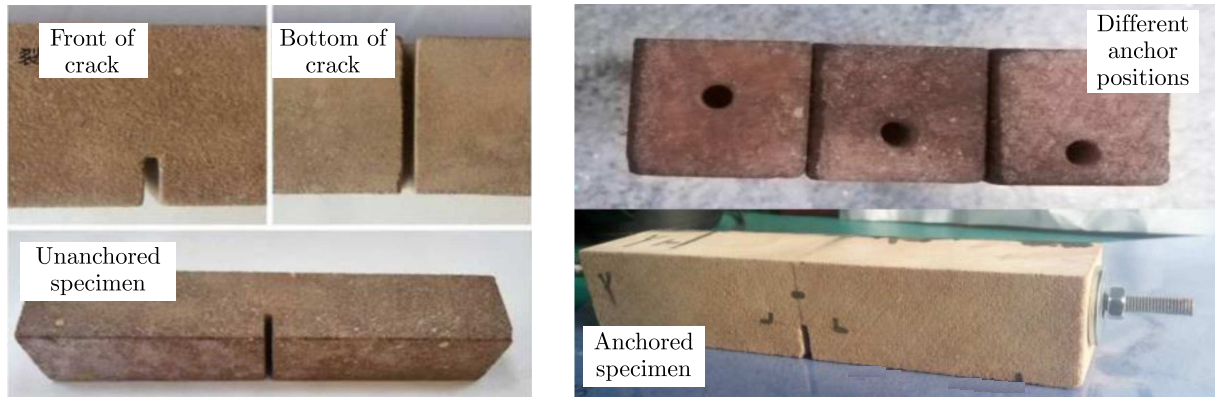
Fig. 3. Three-point bending specimen

Taking the anchoring position and pre-tightening force as the research variables respectively, according to different distances from the center of the bolt to the bottom end surface of the specimen, three types of pre-crack types are set up: through crack arrangement, crack tip arrangement and advanced crack arrangement, as shown in Fig. 4. 2 specimens for each plan and a total of 6 specimens, are prepared.
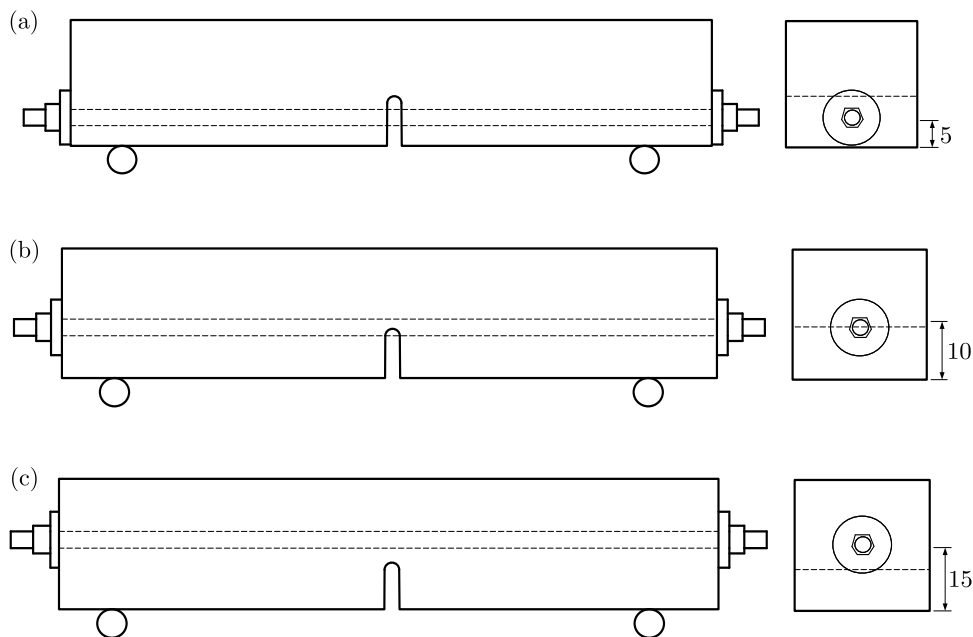

Fig. 4. Anchor position [mm]: (a) through crack arrangement, (b) crack tip arrangement, (c) advanced crack arrangement

In the second plan, while pre-crack anchoring is carried out, five anchor preloads of $0\,\text{kN}$, $0.5\,\text{kN}$, $1\,\text{kN}$, $1.5\,\text{kN}$ and $2\,\text{kN}$ are respectively applied through the tightening nut. Two specimens of each type are prepared, and a total of 10 specimens of all types are prepared. In addition, the three-point bending specimen in this paper is taken from the same red sandstone slab with a thickness of $30\,\text{mm}$, and its basic physical and mechanical parameters are listed in Table 2 through laboratory tests.

2.3. Design of test plan

As shown in Fig. 5, the test uses the RLJW-2000 rock servo pressure testing machine as the axial pressure loading system, and the loading rate is set to $0.03\,\text{mm/min}$ until the specimen

Table 2. Mechanical parameters of red sandstone

Lithology	Density [g/cm^3]	Compressive strength [MPa]	Tensile strength [MPa]	Elastic modulus [GPa]	Bending strength [MPa]
Red sandstone	2.62	62.1	0.46	4.20	3.40

Table 3. Test parameters of specimens

Anchor position	Initial anchoring force [MPa]	Quantity [Piece]	Anchor position	Initial anchoring force [MPa]	Quantity [Piece]
Through crack	0	2	Advanced crack	1.0	2
Crack tip	0	2	Advanced crack	1.5	2
Advanced crack	0	2	Advanced crack	2.0	2
Advanced crack	0.5	2			

breaks. Before the test, the surface of the specimen was polished and the speckle field was sprayed manually. The CCD industrial camera was used for image acquisition at a rate of 15 frames/s. During the test, the YYJ-4/10 clamping extensometer was placed on both sides of the pre--crack, and the anchor rod material was passed through the DH3819Zigbee axial force sensor and fastened with gaskets and nuts to control the pre-tightening force applied by the anchor rod and monitor the anchor rod axial force.
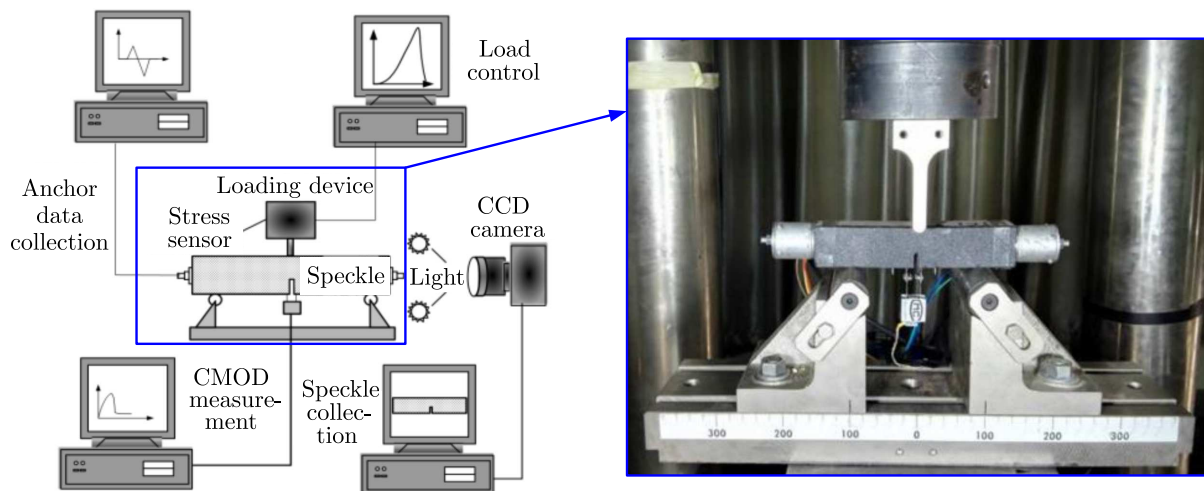

Fig. 5. Test system

In order to monitor the initiation fracture toughness and obtain the crack initiation and propagation law of the prefabricated crack tip, based on the test method in (Peng *et al.*, 2019), a set of resistance strain gauges is arranged at the tip of the prefabricated crack on the back side of the specimen to observe the initiation load P_{ini}.

3. Analysis of test results

3.1. Failure characteristics of anchored sandstone instability

The failure mode of the unanchored specimen is shown in Fig. 6. The rock cracked at the tip of the pre-crack and expanded upward, and the failure mode was mainly the overall fracture

along the pre-crack. Taking into account the heterogeneity and anisotropy of the rock, the crack propagation path and the degree of tortuosity are also different. Some rock cracks do not completely penetrate to the top, but they all present a typical I-type crack fracture mode.
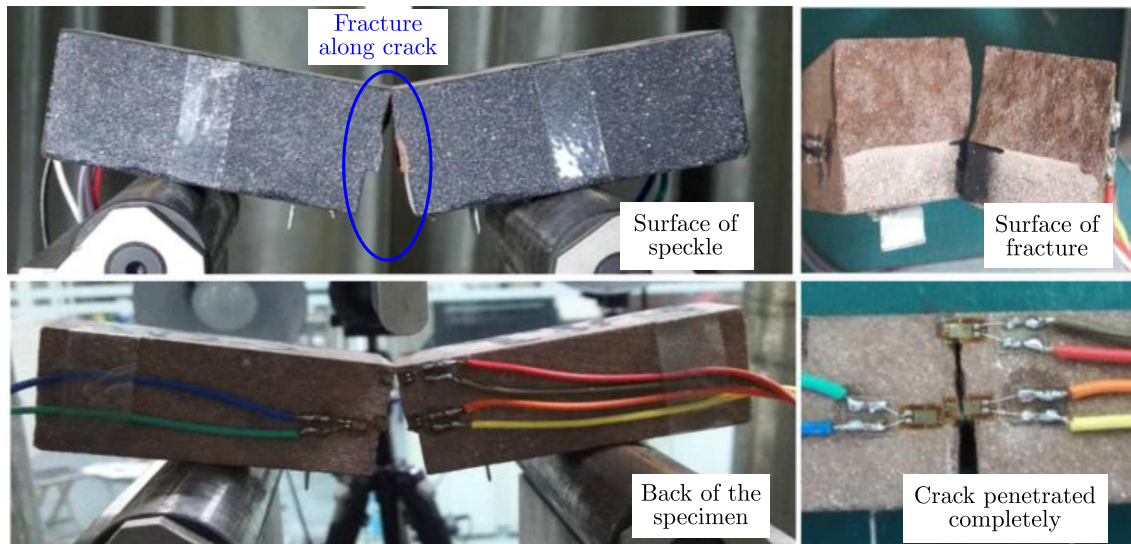

Fig. 6. Failure mode of non-anchor specimen

The failure morphology of the three-point bending-anchored specimen is shown in Fig. 7, which is basically the same as the unanchored specimen. From the tip of the prefabricated crack upward to penetration, a typical type I fracture occurs, indicating that the addition of anchors does not change the overall direction of crack propagation. The threaded rod for anchoring the rock is bent and deformed, and there is an obvious phenomenon of de-threading. The hole in the middle of the specimen is worn by the threaded rod as an ellipse, and the fracture surface produces more debris due to friction and extrusion.
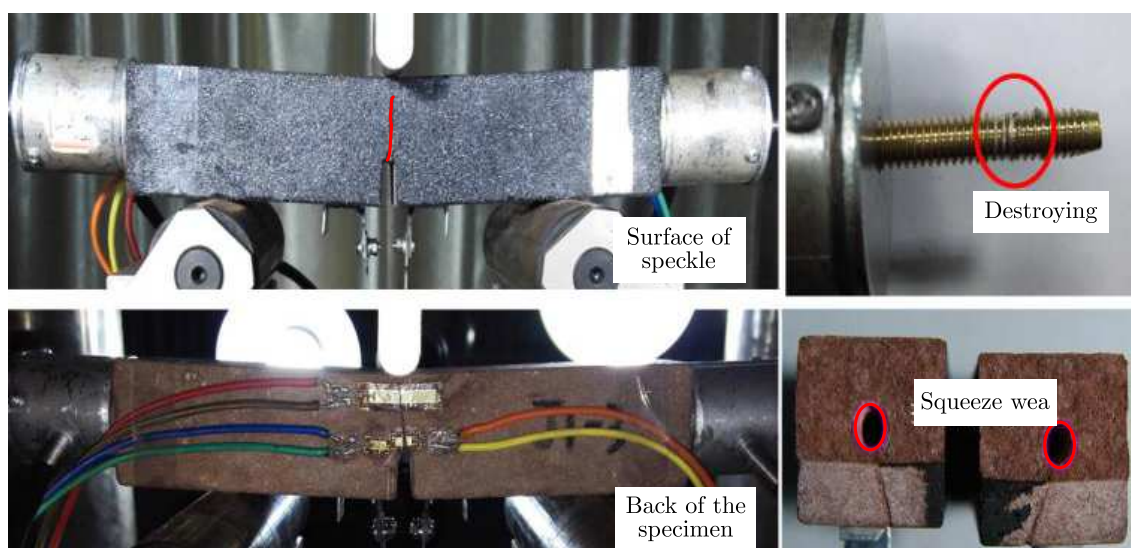

Fig. 7. Failure mode of anchor specimen

3.2. Characteristics of P-$CMOD$ curve

3.2.1. Non-anchor specimen

The P-$CMOD$ curve of the unanchored specimen is shown in Fig. 8. The deformation and failure process of the specimen can be divided into four stages:

(1) In the elastic stage, the opening displacement shows a non-linear increase trend with an increase of the load, and the curve slope turning points A_1, B_1 and C_1 are the crack initiation point;

(2) In the steady-state of crack propagation stage, the crack opening displacement increases faster after the specimen cracks, and reaches the load peak points A_2, B_2, C_2 after the non-linear change ends;

(3) In the instability-state of crack propagation stage, the growth rate of crack opening displacement further accelerates after the load drops from the peak value, and the curve shows a downward trend as a whole;

(4) In the residual stage, the curve goes through the slope turning points A_3, B_3 and C_3, the decline rate slows down, and the crack opening displacement growth rate further increases.
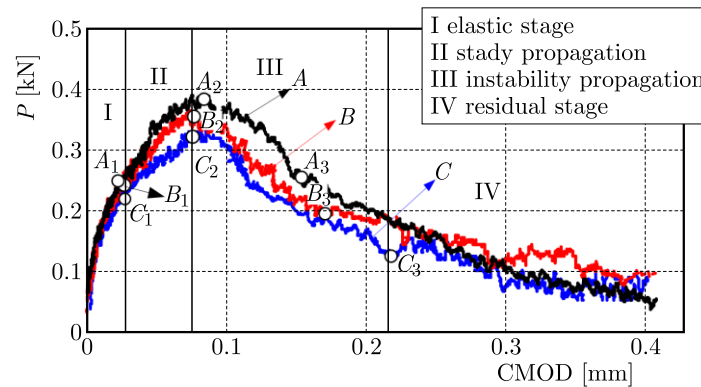

Fig. 8. P-$CMOD$ curve of unanchored sandstone

3.2.2. Specimen with different anchor positions

The P-$CMOD$ curves of the specimens with different anchoring positions are shown in Fig. 9, where Fig. 9b is an enlarged red dotted area of Fig. 9a and a non-anchored contrast curve D is added. The curve of the anchored specimen before cracking basically increases linearly; after the cracking, it enters the stage of stable crack propagation, and the curve changes to a nonlinear growth until it enters the first peak point; after the load drops to 80% P_{max}, it enters the instability expansion stage. The crack opening displacement continues to increase, and the rock enters the crack arrest stage. At this time, the restraint effect of the anchor rod on the rock crack, the closing force of the crack surface and the external load reach a dynamic balance. After the anchor rod bears the main load, it breaks the dynamic balance and enters the crack expansion stage of instability, until the bolt yields.

3.2.3. Anchor specimens with different preload

The P-$CMOD$ curves of the anchored specimens with different pretension forces are shown in Fig. 10, where Fig. 10b is an enlarged view of the red dashed area in Fig. 10a, and a non-anchored specimen curve F is added.

The anchor rod exerts a pre-tightening force to produce a lateral restraint effect on the rock, and the whole can withstand higher external loads before cracking. Therefore, the elastic phase of the P-$CMOD$ curve and the nonlinear phase after the cracking are significantly extended
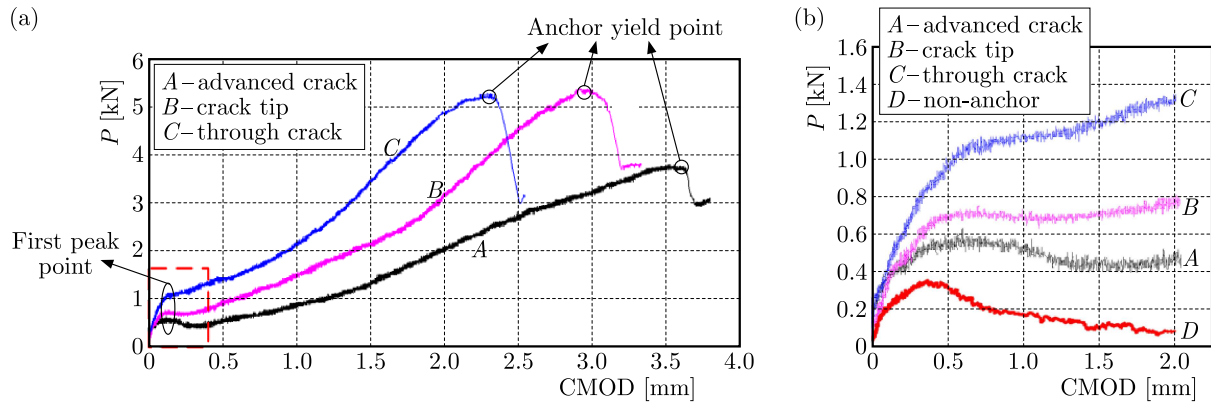
(a)

(b)

Fig. 9. *P-CMOD* curve of anchored rock at different anchor positions: (a) *P-CMOD* curve, (b) partial zoom
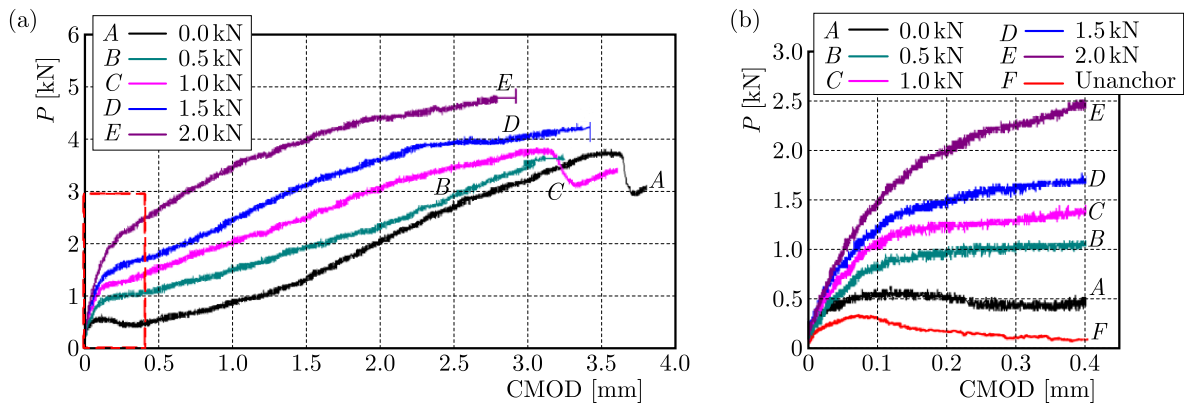
(a)

(b)

Fig. 10. *P-CMOD* curve of anchored specimen with different preload: (a) *P-CMOD* curve, (b) partial zoom

and follow the initial pre-tightening force while it rises and increases. The cracking load is also higher than that of the anchored rock without pretension. After the external load reaches the first peak value, the rock enters the anchor crack arrest stage. The slope of the *P-CMOD* curve increases first and then decreases with an increase of the preload, until it finally stabilizes at the ultimate yield strength of the anchor.

3.3. Fracture parameter characteristics

3.3.1. Non-anchor specimen

After obtaining the unanchored rock initiation load, instability load and displacement of the pre-crack opening in the test, substitute formulas (2.2) and (2.3) to obtain the critical effective crack length, initiation fracture toughness and instability fracture toughness, shown in Table 4. The average fracture toughness of initiation is $0.26\,\text{MPa}\sqrt{\text{m}}$, and the average fracture toughness of instability is $0.48\,\text{MPa}\sqrt{\text{m}}$.

Table 4. Fracture parameters of sandstone unanchored

No.	P_{ini} [kN]	P_{un} [kN]	$CMOD_0$ [mm]	$CMOD_c$ [mm]	a_c [mm]	K_{Ic}^{ini} [MPa$\sqrt{\text{m}}$]	K_{Ic}^{un} [MPa$\sqrt{\text{m}}$]
W0-1	0.249	0.384	0.0169	0.0894	9.88	0.27	0.50
W0-2	0.246	0.356	0.0172	0.0812	9.86	0.25	0.46
W0-3	0.226	0.328	0.0156	0.0790	9.92	0.26	0.48

3.3.2.   Specimen with different anchor positions

The calculated critical effective crack length, initiation fracture toughness, unstable fracture toughness and other parameters are listed in Table 5.

Table 5. Fracture parameters of sandstone with different anchor positions

No.	P_{ini} [kN]	P_{un1} [kN]	P_{un2} [kN]	$CMOD_0$ [mm]	$CMOD_{c1}$ [mm]	a_c [mm]	K_{Ic}^{ini} [MPa$\sqrt{\mathrm{m}}$]	K_{Ic}^{un} [MPa$\sqrt{\mathrm{m}}$]
W1-1	0.258	0.572	3.648	0.0198	0.1087	12.90	0.252	0.666
W1-2	0.248	0.626	3.922	0.0188	0.1198	13.27	0.258	0.710
W2-1	0.436	0.708	5.312	0.0191	0.1333	12.93	0.337	0.814
W2-2	0.300	0.662	4.304	0.0189	0.1000	12.62	0.329	0.767
W3-1	0.454	0.880	5.232	0.0201	0.1112	11.58	0.389	0.894
W3-2	0.422	1.034	5.808	0.0211	0.1387	11.46	0.404	0.986

Compared with the unanchored specimens, the crack initiation and instability fracture toughness of the anchored rock are improved, and the degree of the improvement is related to the anchor rod position. The penetration crack anchoring effect is the most obvious, followed by the crack tip anchoring and the leading crack anchoring. Among them, the fracture toughness of the advanced crack, crack tip and through crack anchoring is increased by 24.4%, 62.4% and 93.7%, respectively; the instability fracture toughness is increased by 69.5%, 94.8% and 131.5%, respectively.

3.3.3.   Specimen with different preload

The initiation and instability loads and the initiation and instability fracture toughness parameters of the anchored rocks with different preloads are listed in Table 6.

Table 6. Fracture parameters of sandstone with different preload

No.	P_{ini} [kN]	P_{un1} [kN]	P_{un2} [kN]	$CMOD_0$ [mm]	$CMOD_{c1}$ [mm]	a_c [mm]	K_{Ic}^{ini} [MPa$\sqrt{\mathrm{m}}$]	K_{Ic}^{un} [MPa$\sqrt{\mathrm{m}}$]
J1-1 (0 kN)	0.258	0.572	3.648	0.0198	0.1087	12.90	0.252	0.666
J2-1 (0.5 kN)	0.744	1.072	3.786	0.0537	0.1600	12.87	0.316	0.754
J3-1 (1 kN)	1.008	1.144	3.786	0.1288	0.2356	11.71	0.399	0.883
J4-1 (1.5 kN)	1.388	1.444	3.894	0.1366	0.1809	12.75	0.455	0.952
J5-1 (2 kN)	1.816	1.934	5.692	0.1350	0.1887	11.20	0.502	1.101

The rock initiation load, crack opening displacement and fracture toughness of initiation are all increasing with an increase of the preload. When the preload increases from 0 kN to 2 kN, the fracture toughness of initiation is higher than that of the unanchored rock. The increments by 24.4%, 55.8%, 97.1%, 129.1%, 151.7%, and 0%, 25.9%, 59.2%, 85.1%, 102.7%, respectively, compared to purely leading crack anchored rock, indicate that the increasing of the pre-tightening force can significantly delay the rock cracked.

The rock instability load and instability fracture toughness tend to increase with an increase of the preload. When the preload increases from 0kN to 2 kN, the instability fracture toughness increases by 69.5%, 93.3, 120.7%, 151.5%, and 182.3%, respectively, compared with the unanchored rock, which are respectively 0%, 14.1%, 30.2%, 48.4%, 66.6% higher than the purely advanced crack anchored rock. The above shows that the fracture toughness of crack initiation and instability increases with growth of the preload. At the same time, when the preload increases to a certain extent, the rock would transform from brittle failure to ductile failure.

4. Conclusion

- The *P-CMOD* curve of the rock three-point bending specimen can be divided into four stages:

  (1) The elastic stage, the curve grows linearly;

  (2) The steady-state crack propagation stage, the curve shows a nonlinear growth with a decreasing slope;

  (3) The crack instability growth stage, the curve decelerates and falls;

  (4) In the residual stage, the curve shows a gentle downward trend.

- In the elastic stage, the horizontal deformation of the rock is less than 0.001 mm and the distribution is irregular. The horizontal deformation of the rock is distributed symmetrically along the crack process area in the steady-state propagation stage and concentrated at the crack tip. The horizontal deformation concentration of the rock crack tip increases and accelerates upward in the unstable propagation stage. The horizontal deformation increment of the rock in the residual stage increases, and the deformation concentration area expands.

- After the anchored rock loses stability, the anchor rod bears the main load, and the crack re-enters the steady-state propagation stage until the anchor rod yields and reaches the secondary instability. The *P-CMOD* curve of anchored rock with low pretension reaches its peak and shows a decelerating and decreasing trend, and the descent speed is positively correlated with the preload. The *P-CMOD* curve of anchored rock with high pretension reaches its first peak and does not fall anymore. It continues the increase and enters the steady-state crack propagation stage. The first peak load increases as the anchoring position moves downward.

References

1. ALIHA M.R.M., SAGHAFI H., 2013, The effects of thickness and Poisson's ratio on 3D mixed-mode fracture, *Engineering Fracture Mechanics*, **98**, 1, 15-28

2. ALIHA M.R.M., BAHMANI A., AKHONDI S., 2016, Mixed mode fracture toughness testing of PMMA with different three-point bend type specimens, *European Journal of Mechanics – A/Solids*, **58**, 148-162

3. DAI S., MA S., PAN Y., DONG Z., 2012, Evaluation of mode I stress intensity factor of rock utilizing digital speckle correlation method, *Chinese Journal of Rock Mechanics and Engineering*, **31**, 12, 2501-2507

4. DENG C.F., LIU J.F., CHEN L., LI Y., XIANG G., 2016, Fracture mechanical behaviors and acoustic emission characteristics of Beishan granites with different particle sizes, *Chinese Journal of Rock and Soil Mechanics*, **37**, 8, 2313-2320

5. DENG C.F., LIU J.F., CHEN L., LI Y., XIANG G., 2017, Mechanical behaviors and acoustic emission characteristics fracture of granite under different moisture conditions, *Chinese Journal of Geotechnical Engineering*, **39**, 8, 1538-1544

6. DING J., LIU J., LI C., YI H., 2013, Failure mechanism of layered salt rock in three-point bending test, *Applied Mechanics and Materials*, **256-259**, 48-56

7. FUNATSU T., SETO M., SHIMADA H., MATSUI K., KURUPPU M.D., 2004, Combined effects of increasing temperature and confining pressure on the fracture toughness of clay bearing rocks, *International Journal of Rock Mechanics and Mining Sciences*, **41**, 6, 927-938

8. HU S.W., LU J., FAN X.Q., 2011, The fracture of concrete based on acoustic emission, *Advanced Materials Research*, **80-81**, 8, 261-265

9. JENABIDEHKORDI A., 2019, Computational methods for fracture in rock: a review and recent advances, *Frontiers of Structural and Civil Engineering*, **13**, 2, 273-287

10. JI W.-W., PAN Z.-P., MIAO S.-T., SU F.-S., DU M.-P., 2016, Fracture characteristics of two type of rock based on digital image correlation, *Chinese Journal of Rock and Soil Mechanics*, **37**, 8, 2299-2305

11. MA S.P., ZHOU H., 2008, Surface strain field evolution of rock specimen during failure process, *Chinese Journal of Rock Mechanics and Engineering*, **27**, 8, 1668-1673

12. NEJATI M., AMINZADEH A., SAAR M.O., DRIESNER T., 2019, Modified semi-circular bend test to determine the fracture toughness of anisotropic rocks, *Engineering Fracture Mechanics*, **213**, 153-171

13. OLSSON E., JELAGIN D., FORQUIN P.A., 2019, Computational framework for analysis of contact-induced damage in brittle rocks, *International Journal of Solids and Structures*, **167**, 24-35

14. PAKDAMAN A.M., MOOSAVI M., MOHAMMADI S., 2019, Experimental and numerical investigation into the methods of determination of mode I static fracture toughness of rocks, *Theoretical and Applied Fracture Mechanics*, **100**, 154-170

15. PARISIO F., TAROKH A., MAKHNENKO R., NAUMOV D., MIAO X.-Y., KOLDITZ O., NAGEL T., 2019, Experimental characterization and numerical modelling of fracture processes in granite, *International Journal of Solids and Structures*, **163**, 102-116

16. PENG Y., ZHAO J.Z., KARNY S., LI Z., XU F., 2019, Study of delayed creep fracture initiation and propagation based on semi-analytical fractional model, *Applied Mathematical Modelling*, **72**, 700-715

17. SHU B., ZHU R., ZHANG S., DICK J., 2019, A qualitative prediction method of new crack-initiation direction during hydraulic fracturing of pre-cracks based on hyperbolic failure envelope, *Applied Energy*, **248**, 185-195

18. TADA H., PARIS P.C., IRWIN G.R., 2000, *The Stress Analysis of Cracks Handbook*, New York, ASME Press, 39-81

19. WU L., LIU S., WU Y., WU H., 2002, Changes in infrared radiation with rock deformation, *International Journal of Rock Mechanics and Mining Sciences*, **39**, 6, 825-831

20. WANG X., SU O., 2019, Specific energy analysis of rock cutting based on fracture mechanics: A case study using a conical pick on sandstone, *Engineering Fracture Mechanics*, **213**, 197-205

21. XU S.L., REINHARDT H.W., 2000, A simplified method for determining double-K fracture parameters for three-point bending tests, *International Journal of Fracture*, **104**, 2, 181-209

22. ZUO J.P., CHAI N.B., ZHOU H.W., 2013a, Investigation on failure behavior of basalt from different depths based on three-point bending meso-experiments, *Chinese Journal of Rock Mechanics and Engineering*, **32**, 4, 689-695

23. ZUO J.P., ZHOU H.W., FAN X., ET AL., 2013b, Research on fracture behavior of Beishan granite after heat treatment under three-point bending meso-experiments, *Chinese Journal of Rock Mechanics and Engineering*, **32**, 12, 2422-2430